Photophysics of a Xanthenic Derivative Dye Useful as an "On/Off" Fluorescence Probe

Luis Crovetto,[†] Jose M. Paredes,[†] Ramon Rios,[‡] Eva M. Talavera,[†] and Jose M. Alvarez-Pez*[,†]

Department of Physical Chemistry, University of Granada, Cartuja Campus, Granada 18071, Spain, and Department of Organic Chemistry, The Arrhenius Laboratory, Stockholm University, 10691 Stockholm, Sweden

Received: September 10, 2007; In Final Form: October 19, 2007

The photophysical behavior of a new fluorescein derivative has been explored by using absorption and steady-state and time-resolved fluorescence measurements. The influence of ionic strength, as well as total buffer concentration, on both the absorbance and fluorescence has been investigated. The apparent acidity constant of the dye determined by absorbance is almost independent of the added buffer and salt concentrations. A semiempirical model is proposed to rationalize the variations in the apparent pK_a values. The excited-state proton-exchange reaction around the physiological pH becomes reversible upon addition of phosphate buffer, inducing a pH-dependent change of the steady-state fluorescence and decay times. Fluorescence decay traces, collected as a function of total buffer concentration and pH, were analyzed by global compartmental analysis, yielding the following values of the rate constants describing excited-state dynamics: $k_{01} = 1.29 \times 10^{10}$ s^{-1}, $k_{02} = 4.21 \times 10^{8}$ s^{-1}, $k_{21} \approx 3 \times 10^{6}$ M^{-1} s^{-1}, $k_{12}^{B} = 6.40 \times 10^{8}$ M^{-1} s^{-1}, and $k_{21}^{B} = 2.61 \times 10^{7}$ M^{-1} s^{-1}. The decay rate constant values of k_{01}, k_{21}, and k_{21}^{B}, along with the low molar absorption coefficient of the neutral form, mean that coupled decays are practically monoexponential at buffer concentrations higher than 0.02 M and any pH. Thus, the pH and buffer concentration can modulate the main lifetime of the dye.

1. Introduction

Fluorescein in aqueous solution can exist in one or more of four different prototropic forms (cation, neutral, monoanion, and dianion) depending on pH. Moreover, the neutral form presents three additional tautomeric species, namely, lactonic, cetonic, and zwitterionic.[1,2] In the physiological pH range, only the dianion and monoanion forms, with different absorption spectra and fluorescence quantum yields, are important. In the visible range, the absorption maximum of the dianion is at 490 nm. The monoanion has two visible range maxima, one at 454 nm and the other at 474 nm. The extinction coefficients are 8.36×10^4 M^{-1} cm^{-1} for the dianion at 490 nm and 3.03×10^4 and 3.14×10^4 M^{-1} cm^{-1} for the monoanion at 454 and 474 nm, respectively.[3] The maximum excitation wavelength of the dianion at 490 nm, matching the 488 nm spectral line of the argon ion laser, favors its common use as a fluorescent probe. The emission spectra of both the anion and dianion have their maxima around 515 nm. The dianion has a fluorescence quantum yield of 0.93, while for the monoanion, it is 0.37.

Taking advantage of the spectral changes associated with the monoanion−dianion transition, fluorescein has been employed as a pH probe, although for measuring intracellular pH, other dyes such as BCECF [2′,7′-bis(2-carboxyethyl)-5-(and-6)-carboxyfluorescein][4,5] are preferred because they are better retained in cells than fluorescein. BCECF has the additional advantage that its ground-state pK_a is near neutral pH. Nevertheless, BCECF also has some inconveniences such as its high sensitivity to ionic strength due to it having three more carboxylic acid functional groups than fluorescein. The dependence of the apparent ground-state pK_a on the ionic strength (μ) was recently found. The values range from 7.78 at $\mu = 0$ to 6.71 at $\mu = 1.2$.[6]

These above-mentioned spectral changes have also been used to detect DNA hybridization in homogeneous assays.[7,8] The effects of hybridization upon fluorescein monoanion−dianion equilibrium in conjugated fluorescein−DNA were studied by comparing the pH titration profiles of ss-DNA−fluorescein and ds-DNA−fluorescein. The results show that the pK_a of conjugated fluorescein shifts to a higher value when it is in a double-stranded structure. Thus, in the physiological pH range, the relative concentration of conjugated fluorescein molecules in the dianion form is far less in the ds-DNA than that in ss-DNA.[7]

Recently, various fluorescein derivatives called Tokyo Green (TG) have been synthesized, in which methyl or methoxy groups have been introduced into the benzene moiety (one of them replacing the carboxylic group and the other at position 4 or 5).[9] Between these derivatives, 9-[1-(2-methoxy-5-methylphenyl)]-6-hydroxy-3*H*-xanthen-3-one (**TG-I**) (see Scheme 1) has great promise as an on/off fluorescence probe since it is highly fluorescent at basic pH values (anion form of the xanthene moiety), but its quantum yield is near to zero at acidic pH values (protonated form of the xanthene moiety). The absorbance and emission maxima are almost not altered with respect to fluorescein. In addition, it has larger photostability than that of fluorescein and 9-[1-(2-methyl-4-methoxyphenyl)]-6-hydroxy-3*H*-xanthen-3-one (see Figure 1), another TG which is being used as an on/off fluorescence probe.[9,10]

The excited-state proton-transfer (ESPT) reaction of the phenolic group at the xanthene moiety of fluorescein and its derivatives has a peculiar property since the coupled decay of the excited monoanion and dianion can only be achieved if some adequate proton donor/acceptor is present in the medium at a high enough concentration.[3,6,11−13] These ESPT reactions can be inconvenient when fluorescein derivatives are employed as pH probes because an altered environment could itself produce spectral changes independent of the pH. Nevertheless, this

* To whom correspondence should be addressed. Tel.: + 34-958-243831. Fax: + 34-958-244090. E-mail: jalvarez@ugr.es.
[†] University of Granada.
[‡] Stockholm University.

10.1021/jp077249o CCC: $37.00
Published on Web 12/20/2007

property can be seen as an advantage since one can modulate the reaction in the necessary manner.

Although there are some reports on the use of TGs as fluorescence probes, a detailed investigation of their photophysics has not been produced (only values of the quantum yields have been reported). To fully understand the complex photophysics of these new fluorescein derivatives, it is essential to expound on the excited-state dynamics of the molecular forms present at near physiological pH. Rate constants of the excited-state processes and spectral parameters associated with excitation and emission are the relevant parameters to be determined. In addition to the knowledge of their photophysics, these compounds are unique and useful examples for developing a model of two excited-states proton-transfer reactions, donor-/acceptor-mediated, in which one of the implied states is nonfluorescent.

The time-correlated single-photon counting (TCSPC) technique[14,15] supplies time-resolved fluorescence data from which the relevant photophysical parameters can be obtained. To decide on the most suitable model to describe a photophysical system, a multidimensional fluorescence decay data surface is measured under various experimental conditions. For the model of ESPT in the presence of an adequate proton donor/acceptor—covered in this paper—the experimental variables are the excitation (λ_{ex}) and emission (λ_{em}) wavelengths, pH, and buffer concentration C^B. In many instances, single curves of fluorescence decay traces are analyzed in terms of a limited number of decay times τ_i and their associated amplitudes p_i. A more accurate estimation of the τ_i and p_i values can be realized by the global analysis approach in which the decay times τ_i can be linked (e.g., over decay traces for the same sample collected at various emission wavelengths).[16−18] Nevertheless, for decays collected at various excitation wavelengths or pHs, τ_i generally varies and hence cannot be linked. The empirical parameters $\{\tau_i, p_i\}$ are not the primary parameters of interest. The underlying significant parameters, which describe the dynamic behavior of the system, are the rate constants (k_{ij}) defining the excited-state kinetics and spectral parameters related to excitation ($\tilde{b}_1$) and emission ($\tilde{c}_1$). The power of global compartmental analysis (GCA) derives specifically from the fact that it fits directly for these underlying parameters. Indeed, it allows the direct estimation of the parameters of interest from the complete fluorescence decay surface in a single step.[19−21]

Recently, the fluorescence kinetics and the deterministic and the numerical identifiability of the model of the intermolecular ESPT reaction in the presence of adequate proton donor/acceptor (added pH buffer) have been studied.[22] A model is said to be uniquely identifiable if the parameters of the assumed model can be uniquely determined from the idealized experiment. To have a uniquely identifiable model, at least three fluorescence decays should be collected, characterized by at least two different pH values and at least two different nonzero buffer concentrations. In addition to these three traces, a minimum one biexponential fluorescence decay of the pH probe in the absence of buffer has to be recorded to determine all rate constants describing the excited-state events (k_{ij}). Furthermore, for the accurate estimation of k_{ij}, $\tilde{b}_1$, and $\tilde{c}_1$, at least two of these decay traces should be collected at the same pH and excitation and emission wavelengths. It is also advisable to use buffers with pK_a^B values comparable to or somewhat higher than the pK_a of the dye to have a maximal effect on $\{\tau_i, p_i\}$. For our compound, we chose phosphate buffer ($H_2PO_4^-/HPO_4^{2-}$) with a $pK_a^B = 6.82$ at 20 °C.

In this paper, the ground-state equilibrium between the neutral and anionic forms of **TG-I** through absorption measurements is first explored. Second, the influence of the addition of salt and buffer on its apparent acidity constant measured via absorption is investigated. Next, the steady-state emission spectra, upon consecutive additions of phosphate buffer at fixed pH value, is recorded to test the buffer-mediated ESPT reaction. Finally, the excited-state dynamic of the **TG-I** in the presence of phosphate buffer is investigated in detail using global compartmental analysis of the fluorescence decay surface collected as a function of emission wavelength (λ_{em}), pH, and buffer concentration (C^B).

2. Experimental Section

2.1. Materials and Preparation of Solutions. The fluorescent dye 9-[1-(2-methoxy-5-methylphenyl)]-6-hydroxy-3*H*-xanthen-3-one (**TG-I**) has been synthesized by means of the following general procedure. Xanthone diTBDMS ether was prepared according to the literature.[23] Magnesium turnings (10 equiv) were dried under Ar. After the magnesium turnings were cooled to room temperature, a solution of bromobenzene derivatives in freshly distilled THF was added, and the mixture was stirred at 60 °C to yield phenylmagnesium bromide derivatives. The solution was cooled to 0 °C; then, a solution of xanthone diTBDMS ether in freshly distilled THF was added, and the mixture was stirred for 10 min. The reaction was quenched by adding 2 N HCl(aq), and the resulting yellow precipitate was collected by filtration, washed with a small quantity of THF, and dried in vacuo to yield an almost pure product. Further purification by silica gel column chromatography was done as required. The NMR data matched with those described in the literature.[9]

For the preparation of phosphate buffer ($pK_a^B = 6.82$ at 20 °C) solutions, $NaH_2PO_4 \cdot H_2O$ and $Na_2HPO_4 \cdot 7H_2O$ (both Fluka, puriss. p.a.) were used. To adjust the pH of the aqueous solutions (without buffer), 0.01 M solutions of NaOH and $HClO_4$ were used. NaOH (Aldrich, platelets) and $HClO_4$ (Aldrich) were of spectroscopic grade quality. All of the solutions were prepared using Milli-Q water as the solvent. All of the chemicals were used as received without further purification.

A stock solution of **TG-I** (10^{-4} M) in 1.27×10^{-3} M NaOH was prepared using Milli-Q water. Using this stock solution, the concentrations required of **TG-I** in the appropriate concentrations of NaH_2PO_4 or Na_2HPO_4 solutions were prepared. The required volumes of these two solutions were then mixed to reach the pH values used in the experiments. Solutions of **TG-I** for fluorescence measurements were prepared so that the absorbance of the final solutions at λ_{ex} was lower than 0.1. Solutions were kept cool and in the dark when not in use to avoid possible deterioration by exposure to light and heat as occurs in fluorescein. The solutions were not degassed.

For the study of the ionic strength influence on pK_a by means of absorbance experiments, solutions at eight ionic strengths between 0.02 and 0.90 were prepared by adding appropriate concentrations of KCl to a 0.01 M phosphate buffer. For the pK_a^* calculation by means of the steady-state fluorescence methodology, seven solutions in the presence of 1.0 M phosphate buffer and different pH values were prepared. For the time-resolved fluorescence experiments, five *TG-I* solutions were prepared in the absence of buffer, characterized by the pH values of 4.85, 5.09, 6.00, 6.40, and 9.88. In the presence of phosphate buffer ($C^B = 0.02$, 0.10, and 0.25 M), 21 solutions were prepared within the pH range of 5.00−9.00. Three decay traces with 20 000 counts at the peak maximum for each solution at each emission wavelength were recorded.

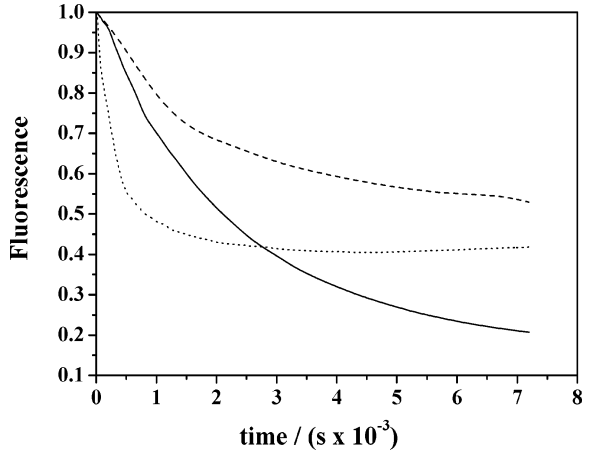

Figure 1. Normalized steady-state fluorescence intensity at 515 nm of viscous solutions of fluorescein (—), **TG-I** (- - -), and **TG-II** (· · ·), continuously irradiated with a Xe lamp (locating the monochromator of the spectrofluorometer at 490 nm and $\Delta\lambda_{ex} = 20$ nm). The ratios of the absorbance at 490 nm from 1×10^{-11} M solutions of **TG-I** and **TG-II** with regard to fluorescein (1×10^{-11} M) were $A_{TG-I}/A_{Fl} = 0.69$ and $A_{TG-II}/A_{Fl} = 0.81$.

2.2. Instrumentation. Absorption spectra were recorded on a GBC Cintra 10e UV/vis spectrophotometer with a temperature-controlled cell holder. The pH of the solutions was measured just before recording each spectrum. All measurements were made at room temperature, using 10×10 mm cuvettes.

Steady-state fluorescence emission spectra were collected on a JASCO FP-6500 spectrofluorometer equipped with a 450 W xenon lamp for excitation, with temperature controller ETC-273T at 20 °C. The pH of the solutions was measured just before the fluorescence measurements at the same temperature.

Fluorescence decay traces of **TG-I** in the absence and in the presence of phosphate buffer were recorded by the single-photon timing method, using the FluoTime 200 fluorometer (PicoQuant, Inc.). The excitation was by a 488 nm laser-pulsed PicoTA (PicoQuant, Inc.), and the observation was through a monochromator at different wavelengths. The pulse repetition rate was 20 MHz. Fluorescence decay histograms were collected in 1320 channels using 10×10 mm cuvettes. The time increment per channel was 36 ps. Histograms of the instrument response functions (using LUDOX scatterer) and sample decays were recorded until they typically reached 2×10^4 counts in the peak channel. The total width at half-maximum of the instrument response function was ~60 ps. Fluorescence decays were recorded at three λ_{em}'s (505, 515, and 535 nm) for all samples.

2.3. Data Analysis of Time-Resolved Fluorescence. The decay traces were individually analyzed in term of exponential models using FluoFit software (PicoQuant, Inc.). The tested decay functions were either monoexponentials or biexponentials. The decay traces of solutions at the same pH, buffer concentration, excitation wavelength, and temperature were globally analyzed by means of the same FluoFit software. The decay times were linked as shared parameters, whereas the pre-exponential factors were local adjustable parameters.

The global compartmental analysis of the fluorescence decay surface of species undergoing excited-state processes in the presence of added buffer was implemented in a general global analysis program using Gaussian-weighed nonlinear least-squares fitting based on Marquardt−Levenberg minimization (see Supporting Information).[24] Any of the fitting parameters can be kept fixed during the fitting or may be freely adjustable to seek optimum values.

3. Results and Discussion

3.1. Photostability. Viscous diluted solutions (1×10^{-11} M) of fluorescein, 9-[1-(2-methoxy-5-methylphenyl)]-6-hydroxy-3*H*-xanthen-3-one (**TG-I**), and 9-[1-(2-methyl-4-methoxyphenyl)]-6-hydroxy-3*H*-xanthen-3-one (**TG-II**) in glycerol as the solvent were irradiated continuously by means of a Xe lamp in order to afflict maximum damage and test their photostability. Figure 1 shows the resulting steady-state fluorescence signal versus time. As can be seen, **TG-I** retains a higher fluorescence signal than the other dyes at the same irradiation times. Therefore, we choose **TG-I** as the reference compound to study the photophysical behavior of the on/off Tokyo Green dyes. It should be noted that **TG-I** solutions as dilute as 1×10^{-10} M were stable after continuous irradiation when they were dissolved in pure (or buffered) water without glycerol.

3.2. Absorption Spectroscopy. *3.2.1. Absorption Measurements and Ground-State Equilibria of **TG-I**.* The visible absorption spectra of aqueous solutions of **TG-I** as a function of pH in the range between 2.71 and 9.12 were recorded. With pH variation, changes in absorbance were clearly observed. The experimental absorption spectra of solutions at different pH values show pH-induced transitions due to ground-state proton reactions, and they occur in regions of pH dictated by the ground-state pK_a values. In Figure 2a, two different isosbestic points can be distinguished; one of them is around 455 nm at low pH values, and the other, at moderate pH values, is shown at 460 nm. For clarity, Figure 2a only contains spectra from six solutions. The absence of the carboxylic group in the benzene moiety of **TG-I**, with respect to the chemical structure of fluorescein and the number of isosbestic points, suggest that **TG-I** in aqueous solution presents three visible absorbing prototropic forms, namely, cation (C), neutral (N), and anion (A). Thus, two ground-state pK_a's are involved in the acid−base transitions. The absorbance maximum of the anion is at 490 nm, whereas the absorption spectrum of **TG-I** in a 7.0 M $HClO_4$ solution (corresponding to the cation form) shows its maximum at 431 nm. According to the chemical structure of **TG-I**, different tautomeric modifications for the neutral species are not possible; however, the carbonyl conjugation with the chemical bonds and electron pairs causes a long resonance delocalization of the electrons. The molecule can be represented by a number of canonical forms; of these, the two more representative are the structures depicted in Scheme 1. The aromatic structure on this scheme should contribute the most to the real structure of the resonance hybrid. Since these charged structures are more stable in aqueous solutions, Scheme 1 is assumed to be an adequate representation of the prototropic forms and acid−base equilibria taken into account in this work.

At the near-physiological pH, only the neutral and anionic forms of **TG-I** are relevant, and the proton-exchange reaction is described by the ground-state acidity constant K_a of the dye. The visible absorption spectra of aqueous solutions of **TG-I** in the pH range between 5.15 and 9.50 have been recorded at various phosphate buffer concentrations. Figure 2b shows an example of the visible absorption spectra recorded for **TG-I** buffered solutions ($C^B = 0.01$ M phosphate) at different pH values. In the basic solution, the spectrum is essentially composed of a band characterized by a maximum at 490 nm and a small shoulder around 460 nm. When the pH decreases, the peak at 490 nm is blue-shifted, and its absorbance value decreases, whereas the shoulder becomes more pronounced. At a pH around 5.00, the spectrum shape changes and is composed of two maxima, one at 480 nm and the other at 448 nm. In the pH range of 5.15−9.50, only one isosbestic point (namely, at

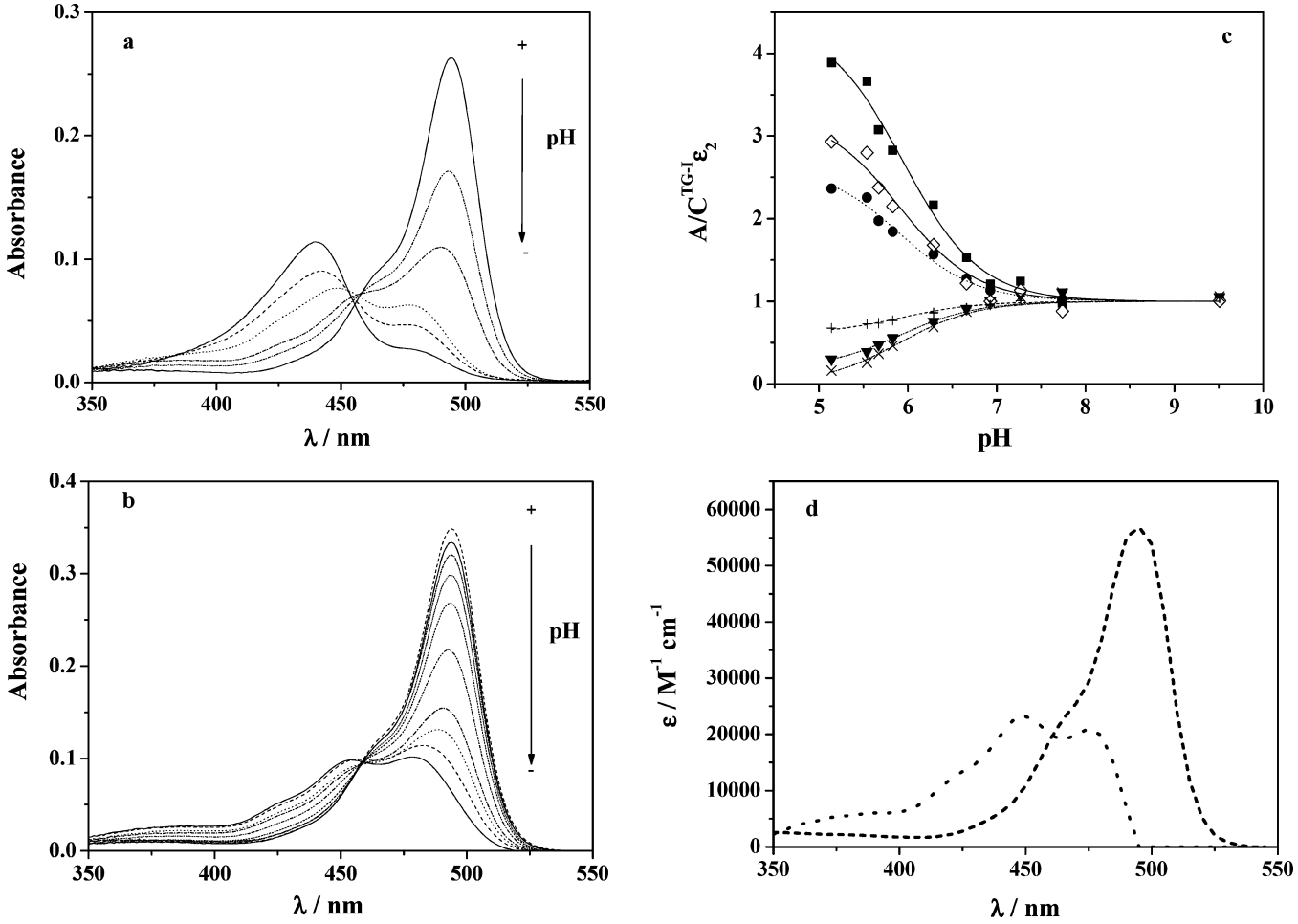

Figure 2. (a) Absorption spectra of 6×10^{-6} M aqueous solutions of **TG-I** at the following pH values: 2.71, 3.20, 3.72, 5.93, 6.70, and 9.12. The arrow indicates decreasing pH values. (b) Absorption spectra of **TG-I** (at 6×10^{-6} M) in phosphate buffer ($C^B = 0.01$ M) at pH values between 5.15 and 9.50. The arrow indicates decreasing pH values. (c) Global fitting of the $A/(C^{TG-I} \times \epsilon_2)$ versus pH curves of **TG-I** solutions in 0.01 M phosphate buffer. The wavelengths shown are 420 (■), 440 (●), 490 (▼), 400 (◊), 475 (+), and 500 nm (×). (d) Recovered molar absorption coefficients of the **TG-I** neutral (· · ·) and anion (- - -) in 0.01 M phosphate buffer.

460 nm) can be clearly distinguished. The experimental absorption spectra of **TG-I** solutions at pH values ranging between 5.15 and 9.50 show that only one pH-induced transition at near-physiological pH (characterized by one ground-state pK_a) is involved. At pH values below 5.15, the isosbestic point disappears, indicating that other different species are involved in the ionic equilibrium. Assuming the acid−base equilibria between the prototropic forms depicted in Scheme 1, the absorption of the phenolate anion of **TG-I** is red-shifted and has an increased molar absorption coefficient relative to the phenolic neutral form, as happens in fluorescein.

The absorbance A of the aqueous solutions of **TG-I** depends on pH according to Beer's law and the simple acid−base equilibrium theory. To analyze the experimental absorbance versus pH, we implemented a global nonlinear least-squares curve fitting method. Assuming that the neutral/anion system follows Beer's law, at any wavelength λ_{abs} and pH, the absorbance A is given by the expression

$$A(\mathrm{pH},\lambda_{abs}) = C^{TG-I}\left(\sum_i \alpha_i(\mathrm{pH},\mathrm{p}K_a^{app})\epsilon_i(\lambda_{abs})\right)d \qquad (1)$$

where C^{TG-I} is the total concentration of **TG-I**, d is the optical path length, $\epsilon_i(\lambda_{abs})$ is the molar absorption coefficient of the ith prototropic form of **TG-I** depending on wavelength, and α_i (pH,pK_a^{app}) is the fraction of **TG-I** in the ith prototropic form. The values of α_i depend on both pH and the apparent ground-state acidity constant (pK_a^{app} value) according to the simple acid−base equilibrium equations.

The nonlinear global fitting of the entire A versus pH versus λ_{abs} surface to eq 1 and the corresponding acid−base equilibrium equations allows the determination of the molar absorption coefficients $\epsilon_i(\lambda_{abs})$ and pK_a^{app}. In this global fitting, the apparent pK_a^{app} was a linked parameter over the whole surface, while $\epsilon_i(\lambda_{abs})$ were locally adjustable parameters at each wavelength for each species. A typical A versus pH versus λ_{abs} data surface at each buffer concentration and ionic strength was composed of 11 pH values, 3 different **TG-I** concentrations, and 100 λ_{abs} values between 350 and 550 nm. The spectra corresponding to pH values lower than 5.15 were removed from the analysis because they did not have the isosbestic point, suggesting a third species is involved in the equilibrium. Beer's law for two prototropic species turned out to be the best model to fit the experimental absorption data. A three-species model resulted in a higher parameter dependency and did not improve the statistical goodness-of-fit parameters. Plots of the individual $A/(C^{TG-I} \times \epsilon_2)$ versus pH curves at different wavelengths and the generated curves from the fitting are shown in Figure 2c. In the data surface fitting process, the estimated parameter values were independent of the initial guesses assigned to these parameters. The recovered molar absorption coefficients ϵ_1 of the neutral and ϵ_2 of the anionic forms were practically independent of the ionic strength. Figure 2d shows, as an

SCHEME 1: Chemical Structures and Ground-State Proton-Exchange Reaction of TG-I Forms, C (cation), N (neutral), and A (anion); the Neutral Form is Represented by Two Resonance Structures

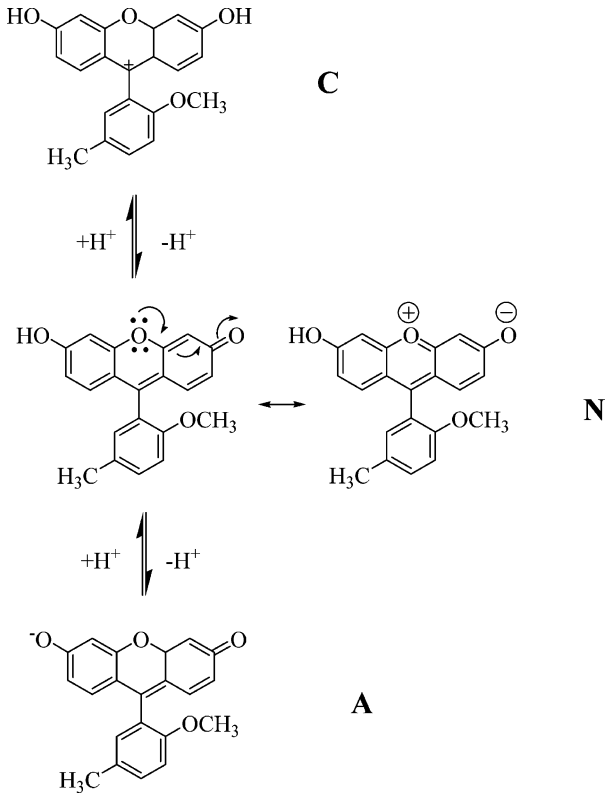

example, the recovered values of the molar absorption coefficients of the neutral and anionic forms in 0.01 M phosphate buffer. The recovered pK_a^{app} values at the different ionic strength studied along with the associated errors are shown in Figure 3.

Since the isosbestic point was consistently around 460 nm at any phosphate concentration, it was concluded that phosphate buffer does not significantly perturb the absorption spectrum of the aqueous **TG-I** solutions, and therefore, this compound does not form ground-state complexes with phosphate buffer.

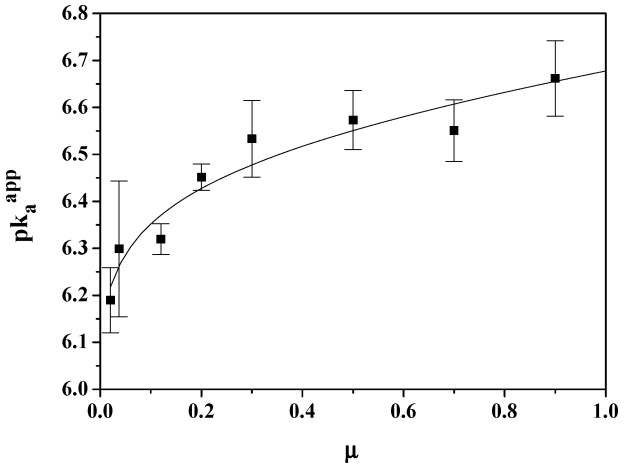

Figure 3. Graphical representation of the dependence of the estimated pK_a^{app} values of **TG-I** on ionic strength (μ). The symbols represent the absorption measurements, and the solid line represents the global fitting of eq 5. The ionic strength values μ were calculated for solutions at 20 °C and pH 6.82 (this pH value corresponds to the pK_a^B value of the phosphate buffer at 20 °C).

3.2.2. Influence of Ionic Strength. The **TG-I** prototropic species of interest are the neutral and the anion. Since the ionic strength affects the ratio of neutral and anion concentrations and, hence, the optical signal from **TG-I**, a comprehensive study of the dependence of K_a on the ionic strength μ is of interest. The Hendersson−Hasselbalch equation, which relates pH with the concentration of the prototropic species, applied to the studied equilibrium of **TG-I** at near-physiological pH, is the following

$$\mathrm{pH} = \mathrm{p}K_a + \log\left(\frac{[\mathrm{A}]}{[\mathrm{N}]}\right) + \log\left(\frac{f_A}{f_N}\right) - \log(a_{H_2O}) \qquad (2)$$

where [N] and [A] represent the concentrations of the neutral and the anion of **TG-I**, respectively, f_N and f_A denote the activity coefficients of these species, and a_{H_2O} is the water activity. The apparent pK_a^{app} is given by

$$\mathrm{p}K_a^{app} = \mathrm{p}K_a + \log\left(\frac{f_A}{f_N}\right) - \log(a_{H_2O}) \qquad (3)$$

and depends on the ratio of the activity coefficients f_i. Since (N) can be either an electrically neutral quinoid structure or a double electrically charged structure, its activity coefficient f_N at low ionic strength would be approximated to 1 or smaller than 1, respectively. The plot of the estimated pK_a values as a function of the ionic strength μ, in Figure 3, shows the increase of the apparent ground-state acidity constant pK_a^{app} value with increasing ionic concentration. A similar effect of ionic strength on the apparent deprotonation constants of various amino acids, in which the change in the electrolyte charge by the reaction of deprotonation was from ± to −, has been found.[25] Hence, N should be a double electrically charged structure, in agreement with the proposed form (see Scheme 1) by elemental qualitative theoretical arguments. Therefore, a semiempirical function based on the extended Debye−Hückel equation was used to relate f_i with μ. Using this approach, the activity coefficients may be represented as

$$\log f_i = \frac{-A_{DH} z_i^2 \sqrt{\mu}}{1 + \dot{a}_i B \sqrt{\mu}} + L_i \mu \qquad (4)$$

In this equation, also called the Truesdell−Jones equation, L_i is an adjustable parameter, typical values for A_{DH} and B at room temperature and atmospheric pressure are 0.51 and 0.33, respectively, $\dot{a}_i$ stands for the ionic radius in Angstroms, and z_i is the ionic charge. Substituting eq 4 into eq 2, and assuming a similar radius for N and A (i.e., $\dot{a}_N = \dot{a}_A = \dot{a}$), leads to

$$\mathrm{p}K_a^{app} = \mathrm{p}K_a - \left(A_{DH}(z_A^2 - z_N^2)\frac{\sqrt{\mu}}{1 + \dot{a}B\sqrt{\mu}} + L^*\mu\right) - \log(a_{H_2O}) \qquad (4)$$

in which L^* represents a composite, adjustable parameter of the individual L_i. The experimental pK_a values were fitted to eq 5 using nonlinear least-squares fitting. A value of 6.0 Å was used for the ionic radius $\dot{a}$. Since the experimental molecular radius of **TG-I** is not available, we built a model of the molecule using the Sybyl program[26] to calculate the size and the molecular radius of the **TG-I** compound. For this purpose, appropriate fragments from the Sybyl libraries were used to build the molecule, and partial atomic charges were calculated by means of the Gasteiger−Marsili method.[27] The Tripos force field[28] was

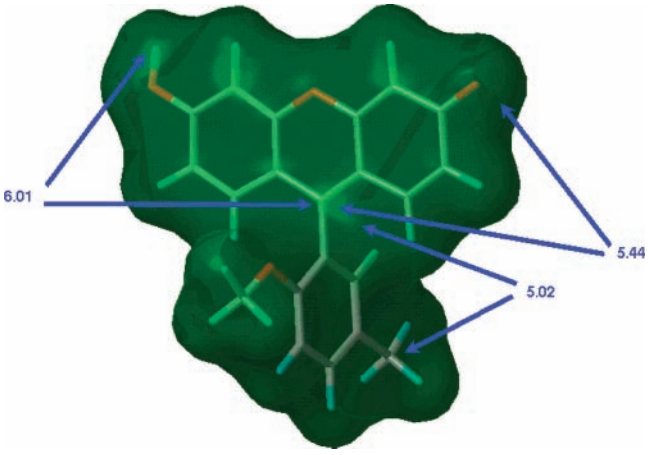

Figure 4. Solvent-accessible surface calculated on the optimized geometry of **TG-I** by means of the Sybyl programs. The value of the surface and the volume calculated are 288.8 Å^2 and 264.7 Å^3, respectively (for the neutral form). Arrows indicate distances measured between the center of mass of the molecule (that almost coincides with C7) and several distal points of the molecule.

used in the energy calculation, and the geometry was optimized using the Powel method,[29] until the energy gradient was smaller than 0.05 kcal mol^{-1} Å^2. Figure 4 represents the solvent-accessible surface on the optimized geometry of **TG-I** calculated by means of the above-mentioned program, as well as some significant distances in the molecule. Calculated values for the surface and the volume of the neutral form of this molecule were 288.8 Å^2 and 264.7 Å^3, respectively (286.8 Å^2 and 263.3 Å^3 for the anion and 291.1 Å^2 and 266.5 Å^3 for the cation). Measured distances between the center of mass (C-7) and several distal points of the molecule range from 5.0 to 6.0 Å, smaller than or equal to the proposed 6.0 Å radius. Since it can be expected that the hydrated radius should be larger than the radius of the same isolated molecule, the average value of 6.0 Å used in the fitting seems to be reasonable. Figure 3 also shows the fitting curve ($r^2 = 0.94$), from which an estimated pK_a value of 6.04 ± 0.03 (at $\mu = 0$) was obtained.

3.3. Emission Spectroscopy. *3.3.1. Buffer-Mediated Excited-State Proton-Transfer Reactions.* Consider a causal, linear, time-invariant, intermolecular system consisting of two different prototropic forms of a ground-state dye and the two corresponding excited-state species, as shown in Scheme 2. For **TG-I** at near-physiological pH, species **1** and **2** are the neutral and anionic form, respectively. Photoexcitation creates the excited-state species **1*** and **2***, which can decay by fluorescence (F) and nonradiative (NR) processes. The composite rate constants for these processes are denoted by k_{01} ($= k_{F1} + k_{NR1}$) and k_{02} ($= k_{F2} + k_{NR2}$). The k_{21} symbolizes the rate constant for the dissociation of **1*** into **2*** and H$^+$. At the pH range considered in this paper, it is assumed that [H$^+$] is so small as to make the rate of association of **2*** + H$^+$ → **1*** negligible. The ground-state proton-exchange reaction is described by the acidity constant K_a of the dye, and the acidity of the buffer can be described by its ground-state acidity constant $K_a^B = [H^+]/[RH]$. In the ground state, the neutral form of the dye (species **1**) can react with the basic form of the pH buffer (R) to give the basic form of the dye (species **2**) and the acidic form of the buffer (RH). In the excited state, the reaction of **1*** with R to form **2*** and RH is characterized by rate constant k_{21}^B. The reverse reaction of **2*** and RH to give **1*** and R is described by rate constant k_{12}^B.

The theory of buffer-mediated ESPT reactions has been well established,[3,6,12,13a] and details of the theory for global bicompartmental analysis and the program implementation procedure are available in the Supporting Information. In brief, if the photophysical system shown in Scheme 2 is excited by an infinitely short light pulse that does not significantly alter the concentrations of the ground-state species, then the fluorescence δ-response function, $f(\lambda_{em},\lambda_{ex},t)$, at emission wavelength λ_{em} due to excitation at λ_{ex}, is given by

$$f(\lambda_{ex},\lambda_{em},t) = p_1 e^{\gamma_1 t} + p_2 e^{\gamma_2 t} t \geq 0 \qquad (6)$$

in which eq 6 has been written in the common biexponential format. The eigenvalues γ_i ($i = 1, 2$) are related to the decay times τ_i ($i = 1, 2$) according to

$$\gamma_i = -1/\tau_i \qquad (7)$$

and are given by

$$\gamma_i = \frac{a_{11} + a_{22} \pm \sqrt{(a_{22} - a_{11})^2 + 4a_{12}a_{21}}}{2} \qquad (8)$$

with a_{ij} as the ijth element of the compartmental matrix **A**

$$\mathbf{A} = \begin{bmatrix} -(k_{01} + k_{21} + k_{21}^b[R]) & k_{12}[H^+] + k_{12}^b[HR] \\ k_{21} + k_{21}^b[R] & -(k_{02} + k_{12}[H^+] + k_{12}^b[HR]) \end{bmatrix} \qquad (9)$$

Therefore, the exponential factors γ_i (and hence also τ_i) depend on pH and the total buffer concentration C^B because [R] and [RH] are generally pH-dependent.

The pre-exponentials, p_i, of eq 6 depend on the rate constants k_{ij}, pH, C^B, and spectral parameters $\tilde{\mathbf{b}}$ and $\tilde{\mathbf{c}}$. The $\tilde{\mathbf{b}}(\lambda_{ex},pH)$ parameters can be expressed as a function of the ground-state acidity constant K_a of the dye, the molar absorption coefficients $\epsilon_i(\lambda_{ex})$ of ground-state species i at λ_{ex}, and the pH of the sample solution. The $\tilde{b}_i$ represents the normalized absorbance of species

SCHEME 2: Representation of the Kinetic Model of Ground- and Excited-State Proton-Exchange Reactions in the Presence of a pH Buffer[a]

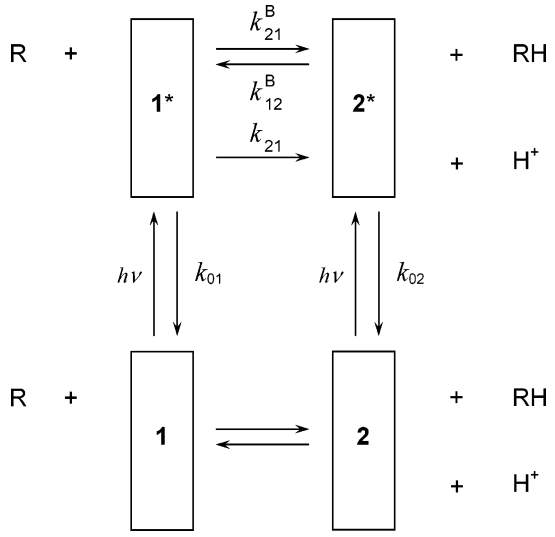

[a] **1** and **2** are, respectively, the ground-state acid (neutral) and conjugate base (anion) forms of the dye **TG-I**, and **1*** and **2*** are the associated excited species. RH and R denote, respectively, the acid and conjugate base forms of the buffer. In the time-resolved experiments of **TG-I**, RH is $H_2PO_4^-$, and R is HPO_4^{2-}. The ground-state forms **1** and **2** of **TG-I** are shown in Scheme 1.

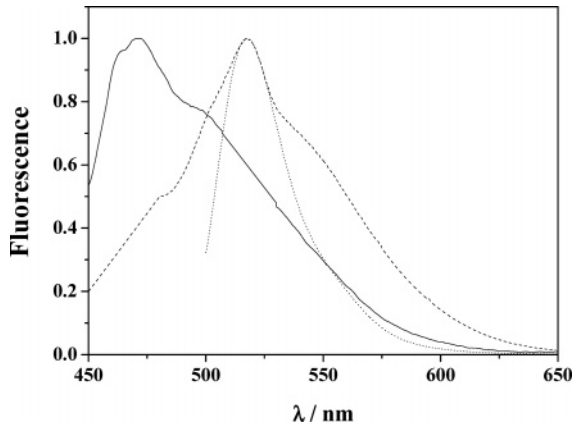

Figure 5. Normalized emission spectra of **TG-I** aqueous solutions at different pH values: (• • •) pH = 9.00; (- - -) pH = 0.52; (—) 7.0 M $HClO_4$. The emission spectrum at pH 9.00 was recorded at λ_{ex} = 490 nm and corresponds to the anion. Both emission spectra at pH 0.78 and 7.0 M $HClO_4$ were recorded at λ_{ex} = 440 nm. These spectra correspond, respectively, to the neutral and cation. Both spectra were multiplied by a factor larger than 300 to show their fundamental characteristics.

i at λ_{ex}, and $\tilde{\mathbf{c}}(\lambda_{em})$ represents the normalized emission weighting factors $\tilde{c}_i(\lambda_{em})$ of species i* at λ_{em}

$$\tilde{c}_i = c_i/(c_1 + c_2) \tag{10}$$

Use of $\tilde{\mathbf{b}}$ and $\tilde{\mathbf{c}}$ in global compartmental analysis allows one to link $\tilde{b}_i$ at the same pH and λ_{ex}, whereas $\tilde{c}_i$ can be linked at the same λ_{em}.

3.3.2. Steady-State Emission Spectra. Although this study is restricted to the near-physiological pH values, the steady-state fluorescence features of aqueous solutions of **TG-I** at any pH are worthy of mention. The steady-state fluorescence emission spectra, at two excitation wavelengths (440 and 490 nm), of aqueous solutions of **TG-I** were recorded over a wide [H^+] range between 7 M $HClO_4$ and pH values up to about 9.00 by using perchloric acid and sodium hydroxide. Only two different spectral profiles were detected in the pH range of 0.78−9.00 (Figure 5). At pH 9.00, only the anion is present, and hence, only this form emits. The anion of **TG-I** has a fluorescence quantum yield around 0.52.[9] It showed an emission band centered on 515 nm, the mirror image of the anion absorption spectrum. The second spectral profile was centered on 515 nm, but it showed a shoulder around 550 nm. It was assumed that this spectral profile corresponds to the neutral form since it was detected at pH values smaller than 3.0. The normalized spectra show that the spectral shape varies only slightly at pHs below 3.0 down to 2.0 M $HClO_4$. Figure 5 shows, as an example, the normalized spectrum at pH 0.78. It should be noted that cation emission was not detected at acid concentrations below 2.0 M, although cation absorption was clearly observed in the [H^+] range between pH 2.71 (see Figure 2) and 2.0 M $HClO_4$. Higher acid concentrations were used to observe the cation emission. Figure 5 also shows the **TG-I** normalized emission spectrum of a 7.0 M $HClO_4$ solution. The spectrum is characterized by an emission band centered at 470 nm along with a shoulder around 500 nm. These features clearly indicate the quick excited-state deprotonation of the cation form. Therefore, the **TG-I** cation can be considered as an enhanced photoacid[30] or "super" photoacid, such as occurs in fluoresceins,[13,31] 8-hydroxypyrene-1,3,6-trisulphonate (HPTS),[32] or cyanonaphtols,[33] showing extremely rapid proton transfer during its excited state. The fact that the **TG-I** cation is such a strong photoacid requires high acid concentrations for detecting the cation emission.[13a] Moreover, it is noticeable that the fluorescence intensities of the spectra corresponding to the neutral and cation forms are very low, and the normalization in Figure 5 was achieved by multiplying by a factor larger than 300.

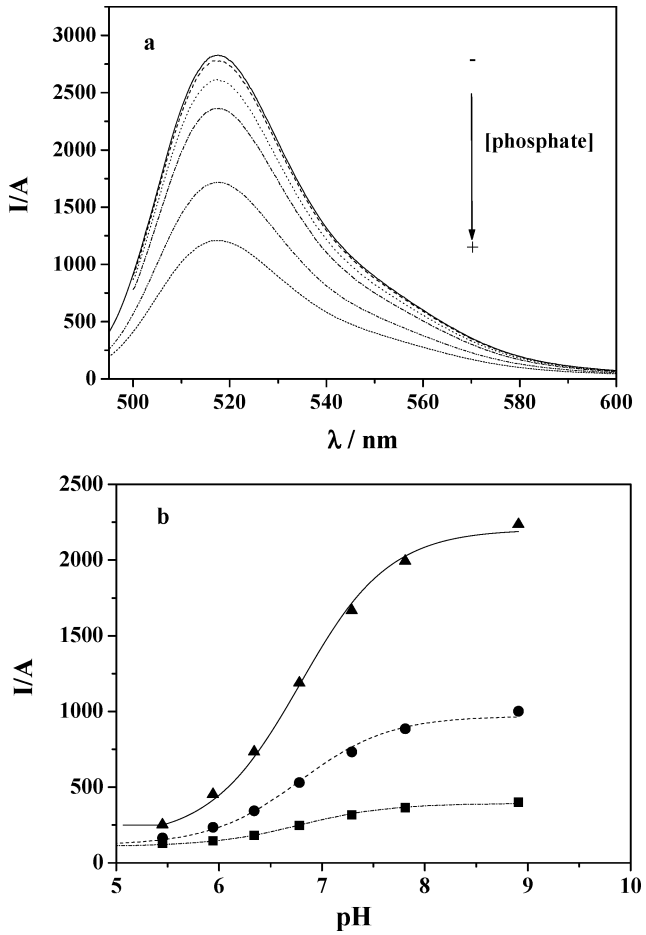

Figure 6. (a) Steady-state emission spectra (λ_{ex} = 490 nm), normalized by the absorbance, of 6 × 10^{-6} M **TG-I** aqueous solutions at different phosphate buffer concentrations, 0.005−1.00 M, and pH 6.78. (b) Plot of the experimental steady-state fluorescence intensity normalized by absorbance (λ_{ex} = 440 (■), 460 (●), and 490 (▲) nm and λ_{em}=515 nm) versus pH, from solutions of 6 × 10^{-6} M **TG-I** and 1.00 M phosphate buffer. Equation 11 was fitted to these experimental values. The lines represent the best fitting curves.

As has been indicated, at near-physiological pH values, only the neutral and anion forms emit, and the **TG-I** emission efficiency is much greater for the anion than that for the neutral form,[9] this being the most important spectral characteristic of the "on/off" fluorescence probes. In Figure 6a, the fluorescence spectra from aqueous **TG-I** solutions in the presence of different concentrations of phosphate buffer (0.005, 0.01, 0.05, 0.10, 0.50, and 1.00 M), at pH 6.78, are shown.

As can be seen, increasing the phosphate buffer concentration resulted in a pronounced decrease in the intensities of the emission band, and this quenching effect saturated at around 1.0 M phosphate buffer. At pH 6.78, the anion/neutral ratio in the ground state is >1, and the 490 nm wavelength almost exclusively excites the more fluorescent anion. Since the neutral form almost does not emit, the emission is dominated by anion emission. Therefore, the experimental results indicate that increasing the phosphate buffer concentration decreases the concentration of excited anion molecules at pH 6.78. Similar results were obtained at the same excitation and emission wavelengths but at lower pH values.

In previous articles, it has been demonstrated that preferential excitation of the lower fluorescent monoanion of fluorescein (or Oregon Green 488) at a pH below the ground-state pK_a values results in the increase of the fluorescence intensity when a suitable proton-donor/-acceptor concentration is present in the medium due to the excited-state proton-transfer reaction that promotes the formation of the more fluorescent dianion.[3,11−13] On the contrary, these current experiments display a different system in which the more fluorescent species is excited. The resulting steady-state emission spectra recorded can be explained as follows: at pH values higher than the ground-state pK_a and 490 nm wavelength, the much more fluorescent **TG-I** anion is preferentially excited; then, the buffer-mediated ESPT reaction rapidly occurs during the excited anion lifetime, forming the nonfluorescent neutral form, and finally, the decays of the two species become coupled. Since the neutral form is not fluorescent and the pH-dependent coupled decay is characterized by a shorter lifetime than that of the anion, the system presents a lower steady-state fluorescence intensity. For this model, the normalized fluorescence intensity can be expressed by[11]

$$\frac{I}{A} = \frac{\phi_1}{1 + 10^{(\mathrm{pH} - \mathrm{p}K_a^*)}} + \frac{\phi_2}{1 + 10^{(\mathrm{p}K_a^* - \mathrm{pH})}} \qquad (11)$$

where I/A is the fluorescence intensity at λ_{em}, normalized by absorbance at the excitation wavelength, ϕ_1 and ϕ_2 are the relative fluorescence efficiencies of the neutral and anion at λ_{em}, and pK_a^* is the pK_a for the excited-state proton reaction $\mathbf{1}^* \leftrightarrows \mathbf{2}^* + H^+$.

Titration graphs of the fluorescence intensity normalized by absorbance versus pH for **TG-I** solutions with a 1.0 M phosphate buffer at pHs between 5.50 and 9.00 (λ_{ex} = 440, 460, and 490 nm; λ_{em} = 515 nm) have been recorded. This plot is shown in Figure 6b. The experimental results of Figure 6b were fitted to eq 11 by nonlinear least-squares estimation, and very good fit parameters were obtained ($r^2 = 0.998$), with a pK_a^* value of 6.78 ± 0.02, similar to the ground-state pK_a^{app} value recovered at high ionic strength. The ϕ_1 and ϕ_2 were floating values during the fitting. The ϕ_1/ϕ_2 ratio obtained at emission wavelengths of 515 nm was 0.08 ± 0.01. This ratio gives an idea of the higher fluorescence efficiency of the anionic form over the neutral form. All of these results, along with the good statistical parameters, show that the excited-state proton-exchange reaction is sufficiently fast to occur during the excited **TG-I** lifetime.

3.3.3. Time-Resolved Emission. Fluorescence decay traces, under different experimental conditions (i.e., absence or presence of phosphate buffer with total concentration C^B and different pH values and λ_{em}) were recorded. First, they were analyzed individually in terms of decay times τ_i and associated pre-exponential factors p_i (i = 1, 2). Such single-curve analysis not only discloses the number of needed exponential terms but also tests the quality of the experimental decay data and allows one to weed out substandard experimental decay data.

Next, classical global analyses in terms of τ_i and p_i were performed, incorporating in a single decay surface the curves collected at the same pH and C^B but at different λ_{em}. The decay times τ_i were linked parameters over decay traces recorded with these characteristics, while pre-exponentials were locally adjustable parameters. It can be expected that such a global analysis would estimate the $\{\tau_i, p_i\}$ values with higher accuracy and precision than single-curve analysis. Finally, all decay traces were analyzed in terms of the rate constants k_{ij} and the spectral parameters $\tilde{b}_1$ and $\tilde{c}_1$ by means of global compartmental analysis.

Individual analyses of traces acquired at C^B = 0 M and pH values between 4.85 and 6.00, measured as a function of λ_{em} (505, 515, and 535 nm), provided good fits with biexponential functions, showing a short decay time around 80 ps and a longer one around 2.36 ns, both pH-independent. Moreover, the shorter decay time had a very small contribution p_1. At pH values larger than 6.00, decays become monoexponential, although keeping their longer lifetime value unchanged with the pH. These results can be explained as follows. Since at C^B = 0 M the buffer-mediated ESPT reaction does not occur to any significant extent, **1*** and **2*** are not coupled and decay independently of each other. At low pH, the ground-state concentration of **1** is much higher than that of **2**, and its lifetime was recovered in the analysis. Due to the large molar absorption coefficient of **2** at λ_{ex} = 488 nm, the anion was also excited and its lifetime recovered too. Unfortunately, the shorter decay time had a very small contribution p_1. Thus, when the solution pH increases, the concentration of the ground-state neutral form decreases. This low concentration along with the low extinction coefficient at the excitation wavelength (488 nm) and the negligible fluorescence quantum yield make the number of fluorescence photons emitted very small from the neutral form of **TG-I**, and the fluorescence decay becomes monoexponential with lifetime τ_2. When the pH is much higher than pK_a, only species **2** and **2*** are present. In that case, the fluorescence decay is given by a monoexponential function characterized by τ_2. Since at those large pH values the protonic concentration is very low, the reprotonation reaction in the excited state is very slow and does not compete with the radiative constant; therefore, this assigns a unique value to k_{02}. On the contrary, the τ_1 lifetime contains the dissociation rate constant k_{21} along with the radiative constant k_{01}; therefore, a unique value to k_{01} from experiments at C^B = 0 cannot be assigned.

Global analysis of the fluorescence decay surface including 45 curves corresponding to C^B = 0 M, in the pH range between 4.85 and 9.88 at λ_{em} = 505, 515, and 535 nm (three decays at each λ_{em}), provided reliable decay time estimates, τ_1 = 0.079 ± 0.004 ns and τ_2 = 2.36 ± 0.01 ns (χ_g^2 = 1.04), corresponding to $(k_{01} + k_{21}) = 1.29 \times 10^{10}$ s^{-1} and $k_{02} = 4.21 \times 10^8$ s^{-1}, respectively. Global curve fitting of those 45 decay curves resulted in the same parameter estimates with the same high precision, regardless of the initial $\{\tau_i, p_i\}$ guesses. The decays at pH > 6.00 were monoexponential, with a lifetime τ_2 corresponding to the anionic form **2***, as predicted by theory.

In order to obviate the ionic strength influence in the apparent acidity constant, the kinetic study has been made at low buffer concentration.[22] Fluorescence decay traces collected at pHs ranging between 5.00 and 9.00 and different C^B values (0.02, 0.10, and 0.25 M) as a function of λ_{em} (505, 515, and 535 nm) were analyzed individually. Only analyses of decay traces recorded from solutions at low phosphate buffer concentrations (C^B = 0.02 or 0.10 M) and pHs ranging between 5.00 and 6.12 were biexponential, providing reliable $\{\tau_i, p_i\}$ estimates. Decay traces collected at larger pH values (and low phosphate buffer concentrations), as well as at any pH and C^B = 0.25 M, did not provide reliable $\{\tau_i, p_i\}$ estimates. That would be caused by the small contribution p_1 of the shorter decay time and could be ascertained from the wide range of $\{\tau_i, p_i\}$ values estimated by the fitting as a function of the initial parameter guesses. Especially imprecise were the values $\{\tau_1, p_1\}$ associated with the shorter lifetime at C^B = 0.25 M, in which the biexponential analyses did not improve the χ_g^2 value, in front of those obtained from monoexponential analyses.

TABLE 1: Rate Constant Values Estimated by Global Compartmental Analysis of the Fluorescence Decay Surface Containing 171 Decay Traces of TG-I in Aqueous Solution in the Absence of Phosphate Buffer (pHs between 4.87 and 9.88) and Presence of 0.02 and 0.10 M Phosphate Buffer (pHs between 5.00 and 9.00)

k_{01} (s^{-1})	$(1.29 \pm 0.03) \times 10^{10}$
k_{02} (s^{-1})	$(4.21 \pm 0.03) \times 10^{8}$
k_{21} (M^{-1} s^{-1})	$(3 \pm 1) \times 10^{6}$
k_{12}^{B} (M^{-1} s^{-1})	$(6.40 \pm 0.41) \times 10^{8}$
k_{21}^{B} (M^{-1} s^{-1})	$(2.61 \pm 0.53) \times 10^{7}$

Global analysis of the fluorescence decay surface, including three decay traces corresponding each surface to one C^B at one pH value and three λ_{em}'s (505, 515, and 535 nm), provided reliable decay time estimates, regardless of the initial guesses. Nevertheless, in a similar way to the individual analyses, only decay traces at low pH values and $C^B \leq 0.10$ M gave biexponential functions with good fitting parameters. The other decay traces at larger pH values than 6.12 and $C^B \leq 0.10$ M, as well as all of the decay traces at $C^B = 0.25$ M, were well analyzed by monoexponential functions, given good fitting parameters ($\chi_g^2 < 1.06$).

Finally, all measured decays (234) were collected in a single decay surface and analyzed globally in terms of the rate constants k_{ij} and the spectral parameters $\tilde{b}_1$ and $\tilde{c}_1$ (by GCA). The linked fitting parameters were k_{01}, k_{02}, k_{21}, k_{12}^B, k_{21}^B, $\tilde{b}_1$, and $\tilde{c}_1$, while the only local (nonlinkable) fitting parameters were the scaling factors κ. This analysis did not result in good fitting statistical parameters. It is known that in order to obtain reliable parameter estimations, it is essential that decays with an unambiguous biexponential nature be used and that the decay times vary considerably as a function of pH and C^B.[22] Thus, data from solutions at any pH and $C^B = 0.25$ M corresponding to decays that gave monoexponential fits in the previous global analyses were removed. With the resulting decay surface composed of 171 decay traces, global compartmental analysis in terms of the rate constants k_{ij} and the spectral parameters $\tilde{b}_1$ and $\tilde{c}_1$ was performed. The rate constants k_{0i} and k_{ij} were linked over the complete fluorescence decay surface. The rate constants k_{12}^B and k_{21}^B were linked over decays in the presence of buffer, whereas they were kept fixed to zero for decays in the absence of buffer. This global fit had $\chi_g^2 = 1.08$ and good residuals and autocorrelation functions. The estimated rate constants are compiled in Table 1. The Supporting Information contains Figure S1 in which two experimental decay traces and the fitting curves provided by the GCA results are shown.

To test the validity of the estimated rate constants, the decay times τ_1 and τ_2 were calculated using the globally estimated rate constant values {k_{01}, k_{02}, k_{21}, k_{12}^B, and k_{21}^B}, C^B, pH, and pK_a^B of phosphate buffer at 20 °C (6.8). A satisfactory agreement between the decay times {τ_2} calculated as a function of pH at $C^B = 0.02$ and 0.10 M and those obtained by global fitting was found, as is shown in Figure 7 in which the decay times {τ_2} obtained by global fitting from decay traces at $C^B = 0.25$ M have also been represented in order to test the deviation between the experimental and calculated values. The agreement is acceptable for the samples at $C^B = 0.25$ M and pH > 6.5. For the samples without an added buffer, a good agreement between the two sets of decay times {τ_1, τ_2} was obtained (calculated values: $\tau_1 = 0.08$ ns and $\tau_2 = 2.36$ ns). The poor correlation between the calculated and estimated τ_1 values as a function of pH and total buffer concentration could be anticipated because it is more difficult to accurately estimate time τ_1 due to its lower contribution and low value. Indeed, its contribution almost vanishes at high pH values and high buffer concentrations.

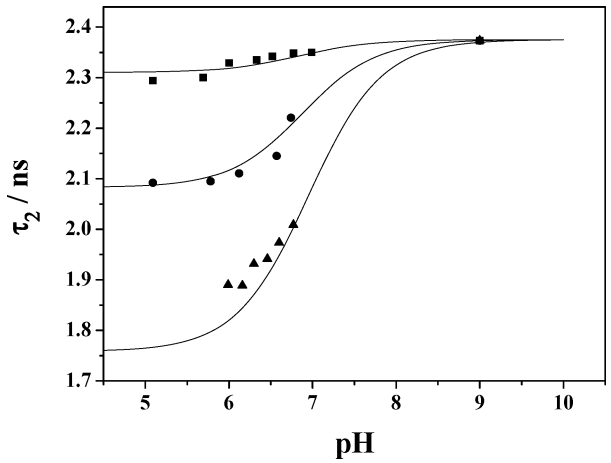

Figure 7. Dependence of the decay times τ_2 on pH at the buffer concentrations of 0.02 (■), 0.10 (●), and 0.25 M (▲). The estimated τ_2 has been obtained by global curve fitting of fluorescence decay surfaces containing three decays collected at each λ_{em} (505, 515, and 535 nm). The decay times (solid lines) have been calculated according to eqs S-3−S-14 using the globally estimated rate constant values {k_{01}, k_{02}, k_{21}, k_{12}^B, k_{21}^B} compiled in Table 1, C^B, pH, and the pK_a^B (6.82) of the phosphate buffer at 20 °C.

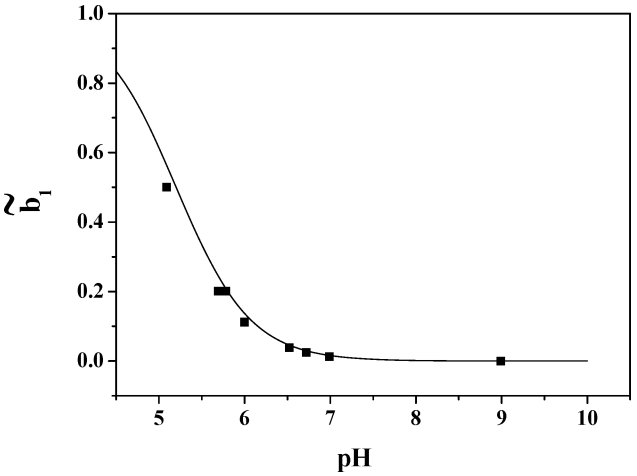

Figure 8. Normalized absorption values $\tilde{b}_1$ of the neutral form of **TG-I** as a function of pH. The black squares represent values estimated by global compartmental analysis. The solid line corresponds to a simulated curve plotted using the eq S-5 and the recovered parameters from the absorption measurements (eq 1).

The values of $\tilde{b}_1$ (normalized absorbance of the neutral **1**) estimated by global compartmental analysis are depicted in Figure 8 as a function of pH. A simulated curve using the $\epsilon_2(\lambda_{ex})/\epsilon_1(\lambda_{ex})$ ratio at $\lambda_{ex} = 488$ nm and K_a values, provided by absorption measurements, is in excellent agreement with the result obtained by global compartmental analysis.

4. Conclusions

The apparent pK_a of the phenolic group in **TG-I** has been obtained by means of absorbance measurements at different ionic strength values. Its dependence on ionic strength has been explored. The increase of the apparent ground-state acidity constant pK_a^{app} value with increasing ionic concentration means that the neutral form should be a double electrically charged structure. However, even a large amount of added buffer does not excessively increase the apparent acidity constant. A simple approach taking into account the variations in the activity factors

was developed, having resolved a semiempirical equation describing the apparent pK_a behavior with ionic strength. Steady-state emission shows that the addition of an adequate buffer results in the ESPT reaction. Time-resolved fluorescence measurements in the absence and presence of phosphate buffer and global compartmental analysis of the fluorescence decay surface have enabled the estimation of the following excited-state rate constants: $k_{01} = 1.29 \times 10^{10}$ s^{-1}, $k_{02} = 4.21 \times 10^{8}$ s^{-1}, $k_{21} \approx 3 \times 10^{6}$ M^{-1} s^{-1}, $k_{12}^{B} = 6.40 \times 10^{8}$ M^{-1} s^{-1}, and $k_{21}^{B} = 2.61 \times 10^{7}$ M^{-1} s^{-1}. These constants display a system in which the experimental conditions of pH and phosphate buffer concentration modulate the value of an only lifetime since the short lifetime contribution almost vanishes at near-physiological pH and high buffer concentrations.

Acknowledgment. This work was supported by Grants CTQ2006-09829 and CTQ2007-61619/BQU both from the Ministerio Español de Educacion y Ciencia and co-financed by the Fondo Europeo de Desarrollo Regional (FEDER). L.C. thanks the University of Granada for a fellowship.

Supporting Information Available: Additional theoretical details for global biocompartmental analysis and the program implementation procedures. This information is available free of charge via the Internet at http://pubs.acs.org.

References and Notes

(1) Zanker, V.; Peter, W. *Chem. Ber.* **1958**, *91*, 572−580.

(2) Diehl, H.; Horchak-Morris, N. *Talanta* **1987**, *34*, 739−741.

(3) Alvarez-Pez, J. M.; Ballesteros, L.; Talavera, E. M.; Yguerabide, J. *J. Phys. Chem. A* ***2001***, *105*, 6320−6332.

(4) Rink, T. J.; Tsien, R. Y.; Pozzan, T. *J. Cell Biol.* **1982**, *95*, 189−196.

(5) Paradiso, A. M.; Tsien, R. Y.; Machen, T. E. *Proc. Natl. Acad. Sci. U.S.A.* **1984**, *81*, 7436−7440.

(6) Boens, N.; Qin, W.; Basarić, N.; Orte, A.; Talavera, E. M.; Alvarez-Pez, J. M. *J. Phys. Chem. A* **2006**, *110*, 9334−9343.

(7) Talavera, E. M.; Alvarez-Pez, J. M.; Ballesteros, L.; Bermejo, R. *Appl. Spectrosc.* **1997**, *51*, 401−406

(8) Talavera, E. M.; Afkir, M.; Salto, R.; Vargas, A. M.; Alvarez-Pez, J. M. *J. Photochem. Photobiol., B* **2000**, *59*, 9−14.

(9) Urano, Y.; Kamiya, M.; Kanda, K.; Ueno, T.; Hirose, K.; Nagano, T. *J. Am. Chem. Soc.* **2005**, *127*, 4888−4894.

(10) Kamiya, M.; Kobayashi, T.; Hama, Y.; Koyama, Y.; Bernardo, M.; Nagano, T.; Choyke, P. L.; Urano, Y. *J. Am. Chem. Soc.* **2007**, *129*, 3918−3929.

(11) Yguerabide, J.; Talavera, E.; Alvarez, J. M.; Quintero, B. *Photochem. Photobiol.* **1994**, *60*, 435−441.

(12) Crovetto, L.; Orte, A.; Talavera, E. M.; Alvarez-Pez, J. M.; Cotlet, M.; Thielemans, J.; De Schryver, F. C.; Boens, N. *J. Phys. Chem. B* **2004**, *108*, 6082−6092.

(13) (a) Orte, A.; Crovetto, L.; Talavera, E. M.; Boens, N.; Alvarez-Pez, J. M. *J. Phys. Chem. A* **2005**, *109*, 734−747. (b) Orte, A.; Bermejo, R.; Talavera, E. M.; Crovetto, L.; Alvarez-Pez, J. M. *J. Phys. Chem. A* **2005**, *109*, 2840−2846. (c) Orte, A.; Talavera, E. M.; Maçanita, A. L.; Orte, J. C.; Alvarez-Pez, J. M. *J. Phys. Chem. A* **2005**, *109*, 8705−8718.

(14) O'Connor, D. V.; Phillips, D. *Time-Correlated Single Photon Counting*; Academic Press: London, 1984.

(15) Boens, N. In *Luminescence Techniques in Chemical and Biochemical Analysis*; Baeyens, W. R. G., De Keukeleire, D., Korkidis, K., Eds.; Marcel Dekker: New York, 1991; pp 21−45.

(16) Knutson, J. R.; Beechem, J. M.; Brand, L. *Chem. Phys. Lett.* **1983**, *102*, 501−507.

(17) Beechem, J. M.; Ameloot, M.; Brand, L. *Anal. Instrum.* **1985**, *14*, 379−402.

(18) Janssens, L. D.; Boens, N.; Ameloot, M.; De Schryver, F. C. *J. Phys. Chem.* **1990**, *94*, 3564−3576.

(19) Beechem, J. M.; Ameloot, M.; Brand, L. *Chem. Phys. Lett.* **1985**, *120*, 466−472

(20) Ameloot, M.; Beechem, J. M.; Brand, L. *Chem. Phys. Lett.* **1986**, *129*, 211−219.

(21) Ameloot, M.; Boens, N.; Andriessen, R.; Van den Bergh, V.; De Schryver, F. C. *J. Phys. Chem.* **1991**, *95*, 2041−2047.

(22) Boens, N.; Basarić, N.; Novikov, E.; Crovetto, L.; Orte, A.; Talavera, E. M.; Alvarez-Pez, J. M. *J. Phys. Chem. A* **2004**, *108*, 8180−8189.

(23) Minta, A.; Kao, J. P. Y.; Tsien, R. Y. *J. Biol. Chem.* **1989**, *264*, 8171−8178.

(24) Program developed jointly by the Technology Institute of the Belarusian State University (Minsk, Belarus) and the Division of Molecular and Nanomaterials of the K. U. Leuven (Leuven, Belgium).

(25) Vilariño, T.; Fiol, S.; Armesto, X. L.; Brandariz, I.; Sastre de Vicente, M. E. *J. Chem. Soc., Faraday Trans.* **1997**, *93*, 413−417.

(26) *SYBYL Molecular Modelling Software*; Tripos Inc.: 1699 S. Hanley Road, St. Louis, MO 63144-2913; http://www.tripos.com.

(27) (a) Gasteiger, J.; Marsili, M. *Tetrahedron* **1980**, *36*, 3219−3222. (b) Gasteiger, J.; Marsili, M. *Org. Magn. Reson.* **1981**, *15*, 353−360.

(28) Clark, M.; Cramer, R. D., III; Van Opdenbosch, N. *J. Comput. Chem.* **1989**, *10*, 982−1012

(29) Powell, M. J. D. *Math. Prog.* **1977**, *12*, 241−254

(30) Tolbert, L. M.; Solntsev, K. M. *Acc. Chem. Res.* **2002**, *35*, 19−27.

(31) (a) Shah, J.; Joshi, N. B.; Pant, D. D. *Curr. Sci.* **1984**, *53*, 255−256. (b) Shah, J.; Pant, D. D. *Curr. Sci.* **1985**, *54*, 1040−1043.

(32) Suwaiyan, A.; Al-Adel, F.; Hamdan, A.; Klein, U. K. A. *J. Phys. Chem.* **1990**, *94*, 7423−7429.

(33) Tolbert, L. M.; Haubrich, J. E. *J. Am. Chem. Soc.* **1990**, *112*, 8163−8165.